CHALMERS
UNIVERSITY OF TECHNOLOGY

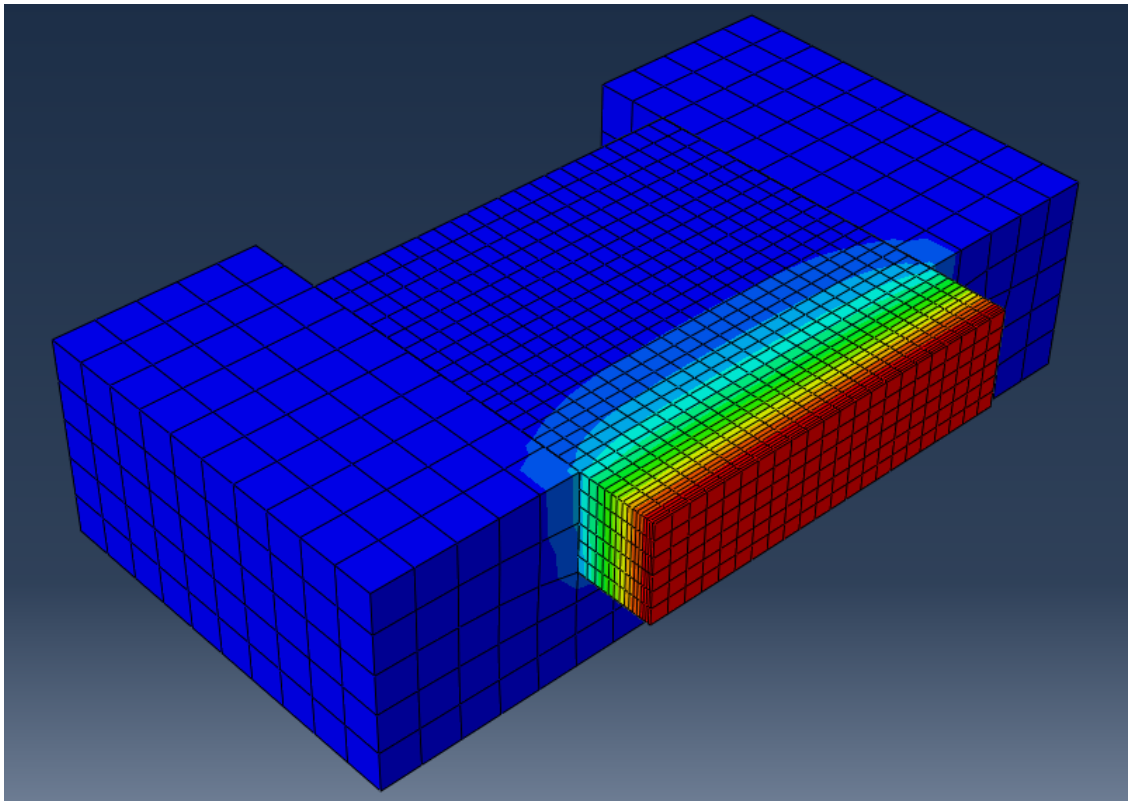

Linear Friction Welding of Rail Materials

Thermal Analysis and Resulting Microstructures of Pearlitic and Bainitic Steels

Research report – Department of Mechanics and Maritime Sciences 2019:04
Part of course *Project in Applied Mechanics* TME131

Johan Andersson
John Ek
Filip Elfving
Jonas Hæg

Supervisors: Moyra McDill, Lennart Josefson

Department of Mechanics and Maritime Sciences
CHALMERS UNIVERSITY OF TECHNOLOGY
Göteborg, Sweden 2019

Linear Friction Welding of Rail Materials

Thermal Analysis and Resulting Microstructures of Parlitic and Bainitic Steels

Johan Andersson
John Ek
Filip Elfving
Jonas Hæg

Supervisors
Moyra McDill
Lennart Josefson

Department of Mechanics and Maritime Sciences
Research report – Department of Mechanics and Maritime Sciences 2019:04
Part of course *Project in Applied Mechanics* TME131
Chalmers university of technology
Göteborg, Sweden 2019

Abstract

Friction welding, a solid state process, is a method that uses heat produced from friction. The produced heat in combination with an external pressure joins the two pieces of material in a weld. Friction welding has several benefits such as lower heat input compared to conventional welding, resulting in a narrower heat affected zone (HAZ), low environmental impact and no melting-solidification phenomena resulting in a structure free of impurities which gives better fatigue properties. These benefits are of particular interest to an ongoing EU-project "Innovative Weld Processes for New Rail Infrastructures" (WRIST).

The present study considers the linear friction welding method (LFW), a method based on relative linear motion of two pieces under compression. A thermal finite element analysis is performed for the LFW process for two different steels, R260 and B360. For the simulations different heat generation models, pressures and welding times are used in different combinations. The microstructure, based on the cooling rates obtained from the simulations, is presented and then validated to experiments. Reaching the microstructures pearlite and bainite and avoiding the microstructure martensite are crucial for the functionality of the resulting weld for both R260 and B360.

It is found that avoiding the formation of martensite is difficult when using the provided welding parameters from the experiments. As a contribution to the WRIST project it is recommended to preheat the material, which was not included in previous experiments. If preheating of the material is considered, it is demonstrated that martensite can be avoided for R260, but not entirely avoided for B360.

Keywords: Linear Friction Welding, Thermal Finite Element Analysis, Microstructure, Preheating, R260, B360

Acknowledgements

We would like to express our very great appreciation to Prof. Emeritus Moyra McDill and Prof. Lennart Josefson, our supervisors, for their valuable and constructive guidance during the planning and development of this project. We would also like to thank Roeland Bisschop and Michele Maglio for supporting us with the model setup in Abaqus and implementation of the heat generation subroutine.

Johan Andersson, John Ek, Filip Elfving, Jonas Hæg, May 2019

Contents

Nomenclature

Abbreviations

Abaqus	Commercial finite element software
B360	Standardised bainite steel
CAD	Computer Aided Design
CCT	Continuous Cooling Transformation
CE	Carbon Equivalent
FE	Finite Element
FEA	Finite Element Analysis
FORTRAN	Programming language
HAZ	Heat Affected Zone
LFW	Linear Friction Welding
MATLAB	Software used for post-processing of data
NDOF	Number of Degrees of Freedom
NEL	Number of Elements
NNODE	Number of Nodes
OFW	Orbital Friction Welding
R260	Standardised pearlite steel
S355JR	Standardised carbon manganese steel
WRIST	EU project *Innovative welding processes for new rail infrastructures*

List of symbols

A	Surface area [m^2]
a	Oscillation amplitude [m]
f	Oscillation frequency [Hz]
h	Heat transfer coefficient [W/(m^2· K)]
P_N	Pressure in welding interface [Pa]
T	Temperature [°C]
T_e	Environmental temperature [°C]
T_s	Surface temperature [°C]
$\bar{q}$	Average heat generation per unit time [W]
q_e	Heat flux to environment [W]
q_f	Heat flux to fixture [W]
q_w	Heat flux from welding [W]
μ	Friction coefficient [-]
σ_y	Yield stress in tension [Pa]
τ	Shear stress [Pa]

List of Figures

List of Tables

1 Introduction

Welding has been used to join railway segments since the beginning of the 19th century [1]. The most used in-track welding method is Aluminothermic Welding of Rails. Molten metal is poured in the gap between the rail segments using a mold. Modelling of this procedure is for example described in Bisschop [2]. After solidification the unnecessary material is removed making the surface of the rail smooth.

An ongoing EU-project "Innovative Welding Processes for New Rail Infrastructures" (WRIST) investigates another method of welding procedure called friction welding. Friction welding, a solid state process, is a method that uses heat produced from friction. The heat, in combination with an external pressure, joins two pieces of material in a weld. Friction welding can be divided into three major methods: rotational, orbital and linear welding. In this study linear friction welding (LFW) of rail steels is considered. The method is based on relative linear motion of the two pieces. This allows components which are nonaxisymmetric to be welded by friction welding [3].

1.1 Background

LFW consists of four phases. In the initial phase, the two pieces are compressed with a pressure load. Then one piece is rubbed against the other as illustrated in Figure 1a. The speed and pressure are such that the friction generates a sufficient amount of heat. In the following transition phase the material in the interface between the two pieces become soft and plasticised and weld flash is produced. The third phase is called the equilibrium phase. In this phase the pieces start to deform. The deformations depend strongly on the temperature in the interface. Clearly an even temperature distribution over the cross-section is required to get an uniform weld. Finally there is a deceleration phase in which the rubbing is immediately stopped, followed by an application of a forging pressure [4]. Figure 1b shows the pieces before and after LFW.

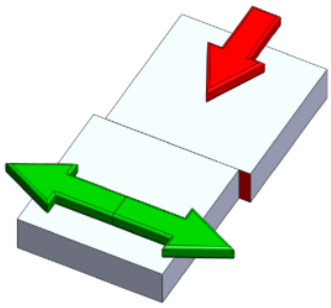

(a) In LFW the linear motion follows the double-headed arrow and the compression pressure is applied at the single-headed arrow. Modified from Faes [5].

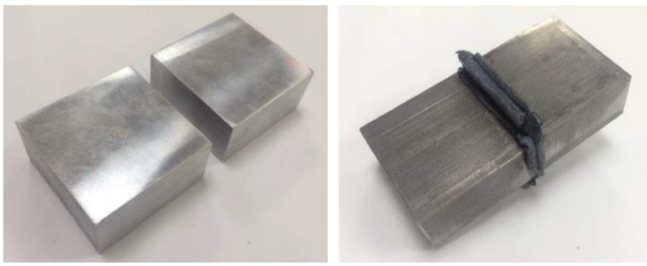

(b) Unwelded and welded (with flash attached) pieces. Modified from Faes [6].

Figure 1: LFW of two pieces

Friction welding has several benefits. The pieces are joined with a lower heat input resulting in a smaller heat affected zone (HAZ), compared to conventional welding [7]. The temperature for which rail steels are considered heat affected is 800 °C, as described in Thorsell [8]. Friction welding joins the parts without melting which gives a structure that is free of impurities, according to Josefson [7]. The material structure is more homogeneous close to the weld region, which gives properties that reduce the susceptibility to fatigue. A problem with the current welding method is that the wear of the rail becomes uneven, due to different microstructures with different hardness in the HAZ. This introduces a bump at the HAZ as the wear becomes uneven. There is interest to investigate LFW within the WRIST project for use in welding rail steels to reduce the width of HAZ.

The heat generated by friction welding is proportional to shear stress and velocity. In LFW the average heat generation $\bar{q}$ per unit time can be modelled as

$$\bar{q} = 4af\tau \tag{1}$$

where τ is the shear stress in the interface cross-section, a is the amplitude of the oscillation motion and f is the oscillation frequency. Hence the oscillation frequency, amplitude and the friction model are the dependent quantities for the generated heat [9]. The product $4af$ corresponds to the average velocity of the welding motion. With sufficient heat input the material can transform into different microstructures i.e, pearlite, bainite, martensite or a combination of these [1], depending on the cooling rate and the rail steel considered.

In the WRIST project two rail steels have been considered: R260 a pearlite steel and B360 a bainitic steel. R260 is the most commonly used rail steel as shown in [10]. B360 is also of interest and has been tested; e.g. on the Paris suburban line where a type of damage called head checks were found in R260 [11]. Both bainite and pearlite are suitable for rails. Martensite is significantly harder and disparities in the hardness of the structure in the rail will, over time, result in irregularities around the weld. A fraction of martensite in the weld which is close to zero is therefore essential for the long term durability of the rail [9]. The three different microstructures are shown in Figure 2.

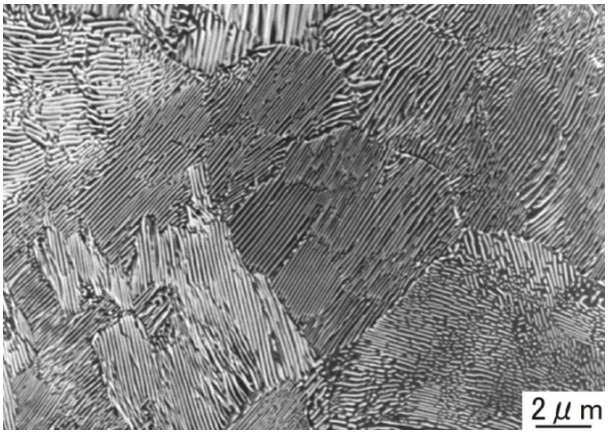

(a) Pearlitic structure [12].

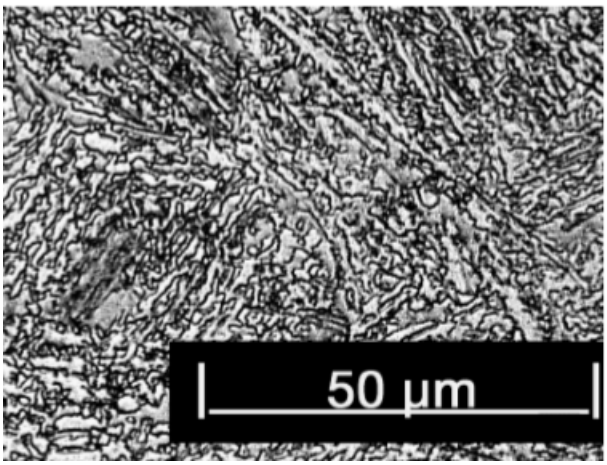

(b) Bainitic structure [11].

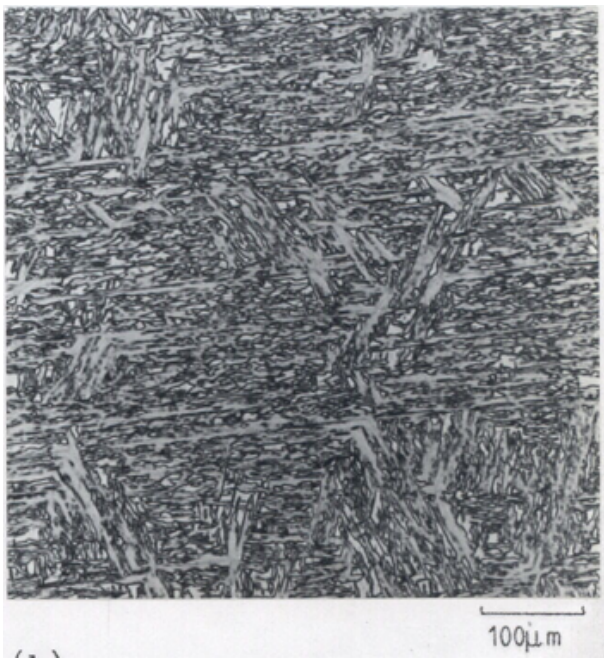

(c) Martensitic structure [12].

Figure 2: Typical microstructures of rail steels.

1.2 Purpose and Approach

Currently R260 with a hardness of 260 HV is the most commonly used railway material. B360 with a higher hardness (360 HV) is used in high performance rails due to its harder surface and better wear resistance.

The purpose of this study is two-fold: first to investigate whether or not LFW will result in a narrow HAZ and second to investigate whether or not LFW of B360, a bainitic steel, can produce a suitable microstructure in the HAZ providing superior properties to R260[1].

The cooling rates from LFW are investigated for R260 and B360. Furthermore this study investigates how these cooling rates affect the transformation to various microstructures. Weld simulations of LFW are compared to experimental data for the R260 and B360 steels. The heat input model is developed so that the calculated temperature fields give microstructures matching those from experimental data for different weld parameters [5]. These results will contribute to the ongoing WRIST project, showing if bainite can be produced by LFW for B360.

1.3 Limitations and Boundaries

The geometry used for comparing simulations to test data is defined by the WRIST project, see Figure 1a. However size and geometry of the fixture and setup of the pieces in the fixture are unknown, i.e how far the piece is sticking out from the fixture.

Conductivity and specific heat for B360 are assumed to be the same as for S355JR, since there are no available thermal properties for this steel. On the other hand the compositions of these two steels are similar. For R260 temperature dependent data points are given [14].

The heat flux models used in this project are given in section 1.3.1, where model 1 has been developed for R260 with OFW. For B360 the same model is used in conjunction with a modified model, called model 2. The temperature dependence of the yield stress, σ_y, used in the heat flux model is limited to a few available data points.

The FE analysis is purely thermal and neglects the influence of mechanical deformations. The material removal during the LFW process is therefore not accounted for.

Significant simplifications in the geometry, heat generation model, material parameters and welding parameters as velocity and pressure are all specified by the WRIST project.

1.3.1 Heat Generation Models

The study was limited to two models to account for the shear stress seen in the heat generation (equation (1)). In the first heat model, the shear stress is proportional to the pressure (coulombfriction) and the friction coefficient has been determined by rotary friction welding experiments for R260 [13], as seen in equation (2). In the second case, the shear stress model is, for lower temperatures, taken as proportional to the pressure and at higher temperatures taken as equal to the yield stress in shear (equation (3)) determined from the von Mises yield criterion.

$$\text{Heat model 1:} \qquad \tau_1 = \mu p_N \tag{2}$$

$$\text{Heat model 2:} \qquad \tau_2 = \begin{cases} \mu p_N & \text{if } \mu p_N \leq \frac{\sigma_y(T)}{\sqrt{3}} \\ \frac{\sigma_y(T)}{\sqrt{3}} & \text{else} \end{cases} \tag{3}$$

For both models the friction coefficient, μ is defined as:

$$\mu = C_1 T^{C_2} e^{C_3 T} \tag{4}$$

where C_1, C_2 and C_3 are constants adopted from experimental data for R260 [13].

[1] R260 has previously been evaluated and shown for rotary friction welding to produce pearlite [13]

2 Method

The heat generated from the linear friction process was calculated using thermal FEA. To solve the FE problem the commercial software Abaqus[2] was used. For the model creation the inbuilt model designer in Abaqus was utilised. For the heat generation model a subroutine script written in FORTRAN was used. Visual Studio[3] is the FORTRAN compiler that was used. All post processing data handling was performed with MATLAB[4].

The temperature was evaluated at the centre line of the weld piece as shown in Figure 4. The first measurement was at the interface with the generated heat flux and the second was at some distance in from the first point, to account for material removal, i.e. burn-off. The work process for the simulations is described below.

- Two heat generation models to predict the amount of heat generated from the linear motion with relative slip velocities in the contact as input were adopted:
  - The first by use of an experimentally fitted model as described in equation 2
  - The second with a temperaturedependent yield stress as described in equation 3
- A thermal FE-model of the welding process was created
- The temperature at the measurement points in the plate, based on the two different heat generation models, was determined and the final microstructures for R260 and B360 steels was estimated.

Two different materials and the two different heat generation models for three different given welding amplitudes (corresponding to three different velocities, since $f = 40\,\text{Hz}$) and three different given burn-off thicknesses (corresponding to three different pressures) resulted in a initial sum of 36 different combinations, see Table 1. After a few simulations a large portion of these combinations were excluded as described in section 3.

Table 1: Parameters for LFW at 40 Hz.

Amplitude [mm]	Burn-off [mm]	Heat model	Material
2, 3, 4	3, 4, 5	Model (1, 2)	R260, B360

The burn-off parameter was translated to pressures and welding times. Three different pressures were given by the WRIST project and welding times between two and seven seconds [6]. The welding time was chosen by this project and includes a longer welding time of eight seconds. The resulting simulation parameters investigated by this project are presented in Table 2. An additional parameter regarding preheating of the specimen was included by this project, which was not included in the experiments [6]. This resulted in a increase of possible combinations from the initial 36.

Table 2: Parameters for LFW at 40 Hz with pressure, welding time and preheating.

Amplitude [mm]	Pressure [MPa]	Weld time [s]	Heat model	Material	Preheating [°C]
2, 3, 4	50, 120, 190	5, 8	Model (1, 2)	R260, B360	200, 350

2.1 Geometry

As illustrated in Figure 1a the welding motion oscillates along the long edge of the cross-section. This corresponds to the designated x-direction. The specimen model has a rectangular cross-section with the dimensions $50\,\text{mm} \times 25\,\text{mm} \times 50\,\text{mm}$ and is a representation of the model used in the experiments. The specimen is attached in a fixture, the part of the specimen sticking out was estimated as 10 mm from a video recording of the experiment provided by Josefson [7]. If the coordinate system is placed in the centre of the specimen, symmetry is obtained about the x-axis. This means that only a half of the specimen needs to be modelled as seen in Figure 3.

[2] Abaqus/CAE, Dassult Systems, version 6.14.2
[3] Microsoft Visual Studio Professional 2013, version 12.0.40629.00 Update 5
[4] MATLAB, version r2018b

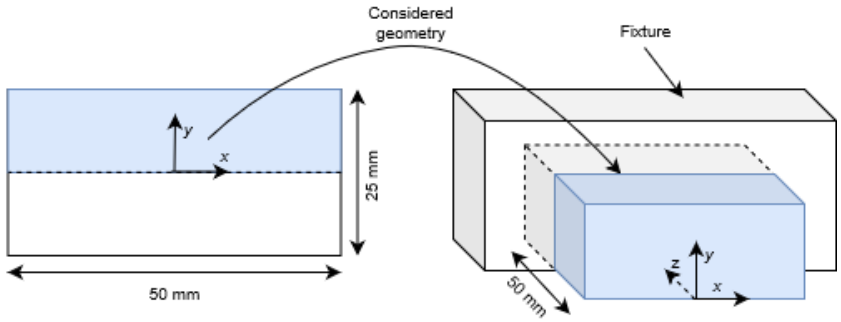

Figure 3: Considered part of the specimen model.

Linear thermal eight-node elements (3D8) were used to model the temperature field. Simulations in orbital friction welding (OFW) have been done previously, allowing mesh convergence to be initialised with a given number of elements (NEL) [15]. Initially the thermal model used approximately 7000 NEL which corresponds to a medium mesh. In order to ensure mesh convergence for LFW, a convergence test was carried out (see Section 2.4). The specimen and the fixture modelled in Abaqus with the used mesh is seen in Figure 4. In the same figure the centre line is defined along which the temperatures will be considered in the post process analysis.

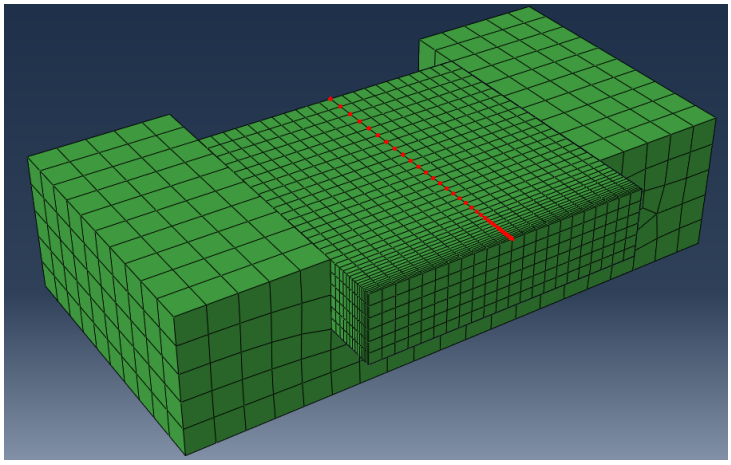

Figure 4: Mesh for the considered model setup. The marked nodes on the symmetry surface are part of the centre line.

2.2 Material Properties

The composition and mechanical properties for the two materials considered in the simulations are presented in Table 3 and Table 6. The thermal properties of conductivity and specific heat are listed in Table 4 and Table 5. For convenience the fixture was the same material as the specimen. The density was assumed to be temperature independent and was set to 7850 kg/m^3 for R260 [14]. The same density was assumed for B360.

Table 3: Compositions for R260 and B360 graded steel [16].

Steel Grade	Composition (Liquid), % by mass						
	C	Si	Mn	P (max)	S (max)	Cr (max)	Cu (max)
R260	0.62-0.80	0.15-0.58	0.70-1.20	0.025	0.025	0.15	-
B360 contains 0.10-0.20% Mo	0.25-0.35	1.00-1.50	1.40-1.70	-	-	0.30-0.70	-
S355JR	0.24	0.55	1.60	0.040	0.040	-	0.55

Table 4: Conductivity and specific heat for R260 [17].

Temperature [°C]	Conductivity [W/mK]	Specific heat [J/kgK]
0	51.9	452
200	48.2	530
400	41.9	610
600	33.9	760
1350	33.9	-
1400	33.9	-

Table 5: Conductivity and specific heat for S355JR [18].

Temperature [°C]	Conductivity [W/mK]	Specific heat [J/kgK]
0	52	480
200	47.5	530
400	42.5	625
700	31	870
800	25	720
1200	30	760

Table 6: Selected mechanical properties for R260 and B360 graded steel [11] [16].

Steel Grade	Fracture Toughness [MPa m1/2]		Max. Fatigue crack growth rate [m/Ge]		Fatigue strength	Residual stress [MPa]	Hardness [HBW]	Tensile strength [MPa]	Elongation [%]	Yield strength [Mpa]
	Min. single value	Min. mean value	Delta K=10 [MPa m1/2]	Delta K=13 [MPa m1/2]						
R260	26	29	17	55	5e8 cycles for total strain amplitude of 0.00135	<250	260-300	880	10	430
B360	36	39	<13	<28	Compliant	<250	360-390	1200	13	850 (min)

CCT diagrams were used for the analyses of the resulting microstructures for the two steels. A CCT diagram illustrates how different cooling rates result in different transformations and the resulting fractions of different microstructures. The CCT diagram for R260 is presented in Figure 5 and the CCT diagram for B360 is presented in Figure 6.

To model the yield stress a standardised material behaviour model described in Euro Code 3 (EC3) was used for R260 [19]. The yield stress was obtained as the reference yield stress at room temperature ($T = 20\,°\mathrm{C}$) multiplied by a reduction factor f_{red}. For B360 the yield stress at room temperature [11] was assumed to be constant from 20 °C to 400 °C. The yield stress at 900 °C and 1200 °C was obtained from experiments [20] and a linear variation between the experimental data points was assumed. A plot showing the variation of yield stress with temperatures from 20 °C to 1200 °C can be seen in Figure 7. For B360 the model was defined by the trilinearisation of the experimental data points. For R260 the model also considered a trilinearisation of the material data which is a simplification of the actual variation.

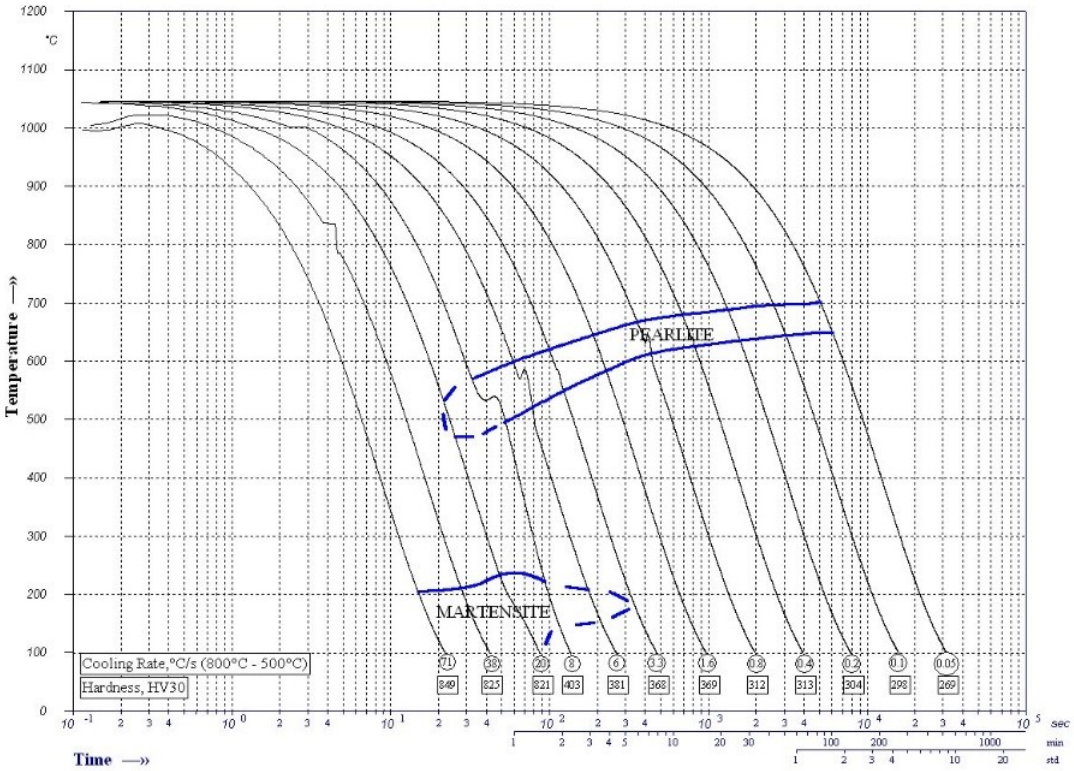

Figure 5: CCT diagram for R260 [7].

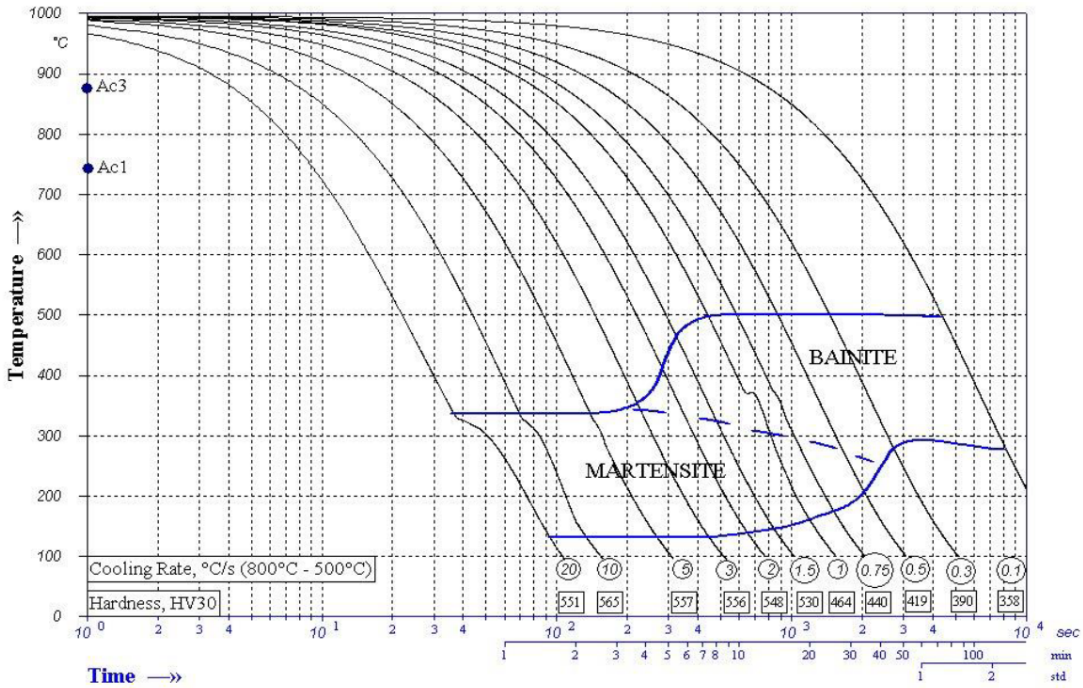

Figure 6: CCT diagram for B360 [7].

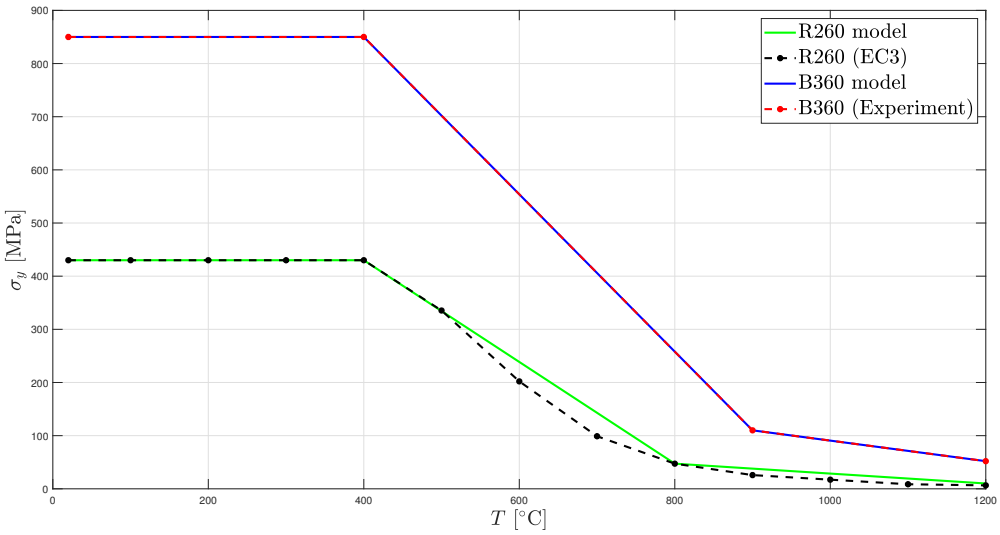

Figure 7: Data and simulation model for the variation of yield strength, σ_y, with respect to temperature for R260 and B360.

Conductivity and specific heat parameters for B360 were not available. Instead parameters for a S355JR steel with similar carbon and manganese composition were used. The S355JR was also used as a surrogate material for B360 for OFW tests in the WRIST project [21]. To motivate this choice the carbon equivalent (CE) for B360 and for SJ355JR was calculated for comparison using the formula of the American Welding Society [22]:

$$CE = \mathrm{C} + \frac{1}{6}\mathrm{Mn} + \frac{1}{5}(\mathrm{Cr} + \mathrm{Mo} + \mathrm{V}) + \frac{1}{15}(\mathrm{Ni} + \mathrm{Cu}) + \frac{1}{6}\mathrm{Si} \tag{5}$$

which results in $CE_{S355JR} = 0.64$ and $CE_{B360} = 0.73$.

As S355JR and B360 are more like carbon-manganese steels (carbon steels containing over 1.2% up to approximately 1.8% manganese [23]) and the CE is sufficiently close, the ability to form martensite is approximately the same.

2.3 Boundary Conditions

The boundary conditions can be divided into three types: natural (Neumann), essential (Dirichlet) and convection boundary conditions (Newton/Robin). At the contact area between the two pieces to be joined a natural boundary condition was applied as a heat flux q_w normal to the cross-sectional surface, see equation (1). The heat flux was a result of the heat generated from the relative movement between the two joining parts. At all other nonsymmetric boundaries, except for the contact surface between the considered geometry and the fixture, a convective heat transfer condition q_e was applied as a function of the room temperature $T_e = 20\,°\mathrm{C}$.

$$q_e = hA(T_e - T_s) \tag{6}$$

h is the heat transfer coefficient for air. It depends on the surrounding air velocity and was set by the WRIST project. A compilation of all boundary conditions included in FEA is illustrated in Figure 8.

The boundary between the welded geometry and the fixture was prescribed by a contact condition, modelling the fixture and welded geometry as one homogeneous solid. Resistance between the pieces was neglected.

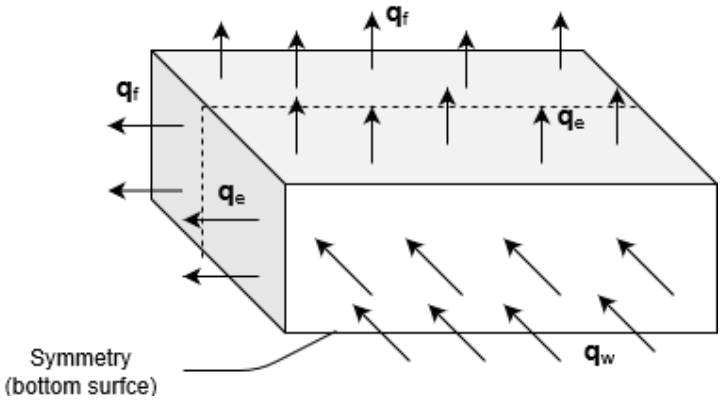

Figure 8: Boundary conditions for the considered geometry.

2.4 Mesh Convergence

A simple mesh convergence test was performed by calculating the temperature field at the centre line of the model. Five different mesh sizes were considered with NEL varying from 323 to 14926 as seen in Figure 9.

There appeared to be no significant difference between the results from the four finest mesh sizes. To clarify this, an error plot was made as shown in Figure 10. The error was computed as the maximum error in temperature between the current mesh and the finest mesh (NEL = 14926) which was assumed to correspond to a converged solution.

The maximum error for the most coarse mesh was about 40 °C and decreased rapidly with increasing NEL. The mesh size used for all further thermal FE-simulations was therefore chosen to consist of 5000 to 6000 elements. The average mesh size and computational costs for the chosen mesh are presented in Table 7.

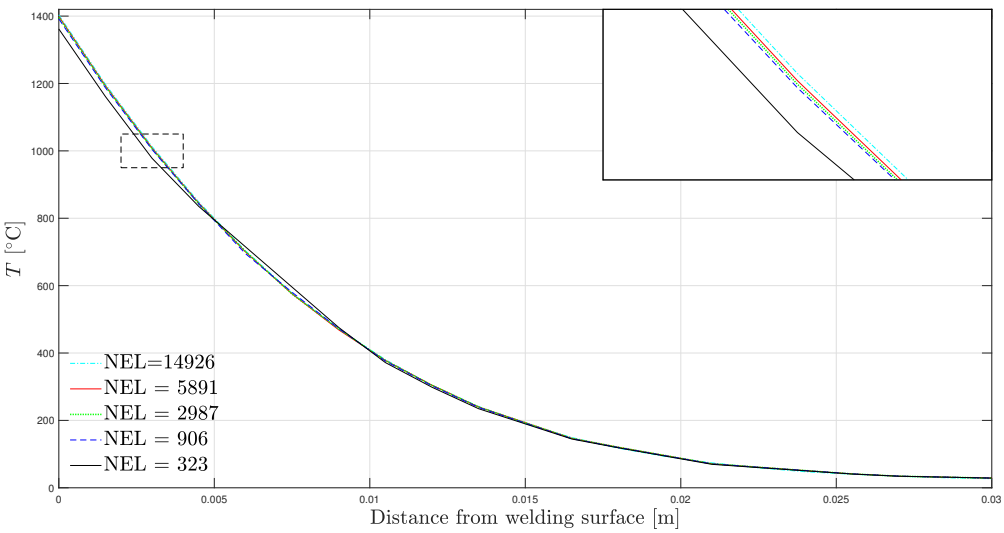

Figure 9: Comparison of temperature fields at centre line for different mesh sizes.

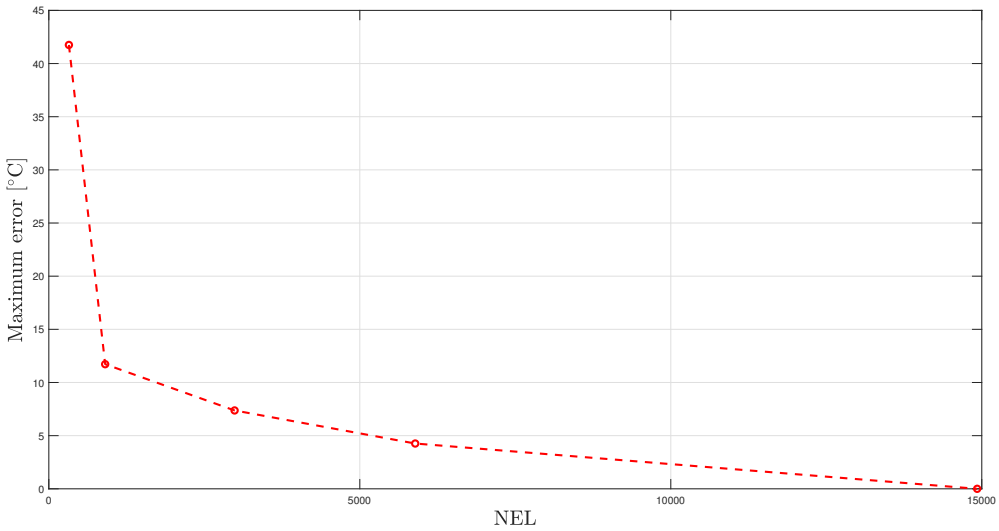

Figure 10: Maximum error from different mesh sizes, compared with converged solution.

Table 7: Mesh size and computational costs.

NEL	NDOF	NNODE	Computational Time [HH:MM:SS]
5351	6860	6860	00:03:13

2.5 Simulation Steps

The FE-simulations were divided into three steps: initial, welding and cooling. In the initial step the temperature of both the fixture and the weld piece was set to 20 °C with no preheating. With preheating the initial temperature was set to 200 °C and 350 °C respectively. The heat flux $\bar{q}$ was applied for 5 s or 8 s during the welding step. Following this step the heat flux was immediately removed and the cooling lasted for 1200 s. Since the shear stress models in equations (2) and (3) are temperature dependent, $\bar{q}$ depends on the solution T via the friction coefficient μ. For each time step $\bar{q}$ was updated with respect to the solution from the previous time step. This was done automatically with scripts written in FORTRAN, found in Appendix A.

2.6 Post Processing

The results from the simulations were extracted from the solution on the centre line, defined in Figure 4, as $T(z(t))$. z is the centre line coordinate with $z = 0$ at the welding surface. For all z, the temperature was identified to get the range of the HAZ. The temperature $T(t)$ was plotted for the coordinate on the edge on the HAZ, i.e the furthest point in the z-direction with a temperature above $800°C$, as well as the coordinate on the welding surface. In order to determine the final microstructure of the weld, $T(t)$ for the cooling step was plotted using the relevant CCT-diagram.

3 Results

The results were characterised in terms of the welding parameters proposed by the project as seen in Table 2 and heat models, for determination of the resulting microstructure and of the approximate HAZ width.

3.1 Parameter Effect of Final Microstructure

Heat model 2 was used for comparing the effect of the pressure, oscillation amplitude, welding time and and surrounding temperature. In section 2.2 the different parameters, given from the WRIST project, are listed. The welding times, pressures and oscillation amplitudes presented in Table 1 are the parameters that were investigated by this project. Some of these parameter tests have been disregarded due to strong trends for pressure, amplitude and welding time. Additional parameters regarding increased welding time and preheating as seen in Table 2 were also used. The parameters affecting the cooling rates the most and consequently the resulting microstructure were seen to be the welding time and preheating for both B360 and R260.

3.2 Comparing Heat Generation Models

All results were evaluated along the centre line of the specimen defined in Figure 4. To make a comparison between the proposed heat generation models the same parameters have been used. In Figure 11 the welding and cooling stages are shown for two different parameter setups. The empirical friction coefficient model is called model 1, see equation (2). Model 2 corresponds to the temperature-dependent yield stress model, see equation (3). Heat model 1 was found to give a bigger difference in the heat input when the pressure and amplitude were increased compared to model 2. The material should not melt fully which suggests that heat model 2 gives a more physically realistic result. Heat model 2 was therefore used for all further simulations. The comparison between the heat models was made for R260 for the parameters seen in Figure 11. Heat model 1 only consider the material parameters and friction coefficients, which are unknown for B360 as no similar experimental model has been developed as for R260. Heat model 2 considers the yield stress which is known for B360 at some temperatures. This is an even more justifiable resolution.

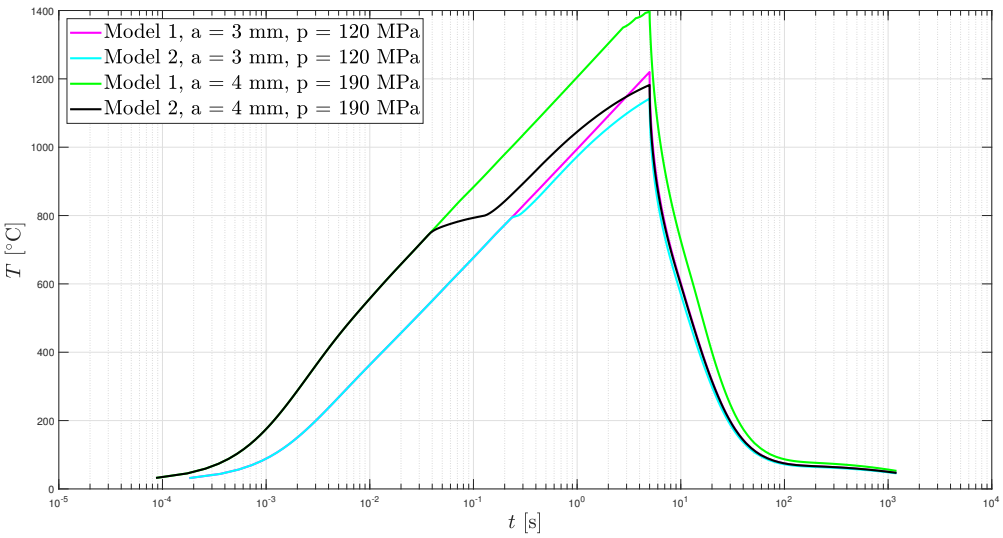

Figure 11: Comparison of the different heat generation models for R260, amplitudes 3 mm and 4 mm, pressures 120 MPa and 190 MPa, welding time 5 s and no preheating, at the welding surface ($z = 0$).

3.3 Estimation of Microstructure for R260

Investigation of the effect of the welding parameters for pressure and oscillation amplitude has been shown to have small impact on the cooling rate. A comparison of cooling rates for different parameters is shown in Figure 12. The maximum values for the pressure and velocity was chosen for all further parameter tests, since they gave the slowest cooling rate within the small variation.

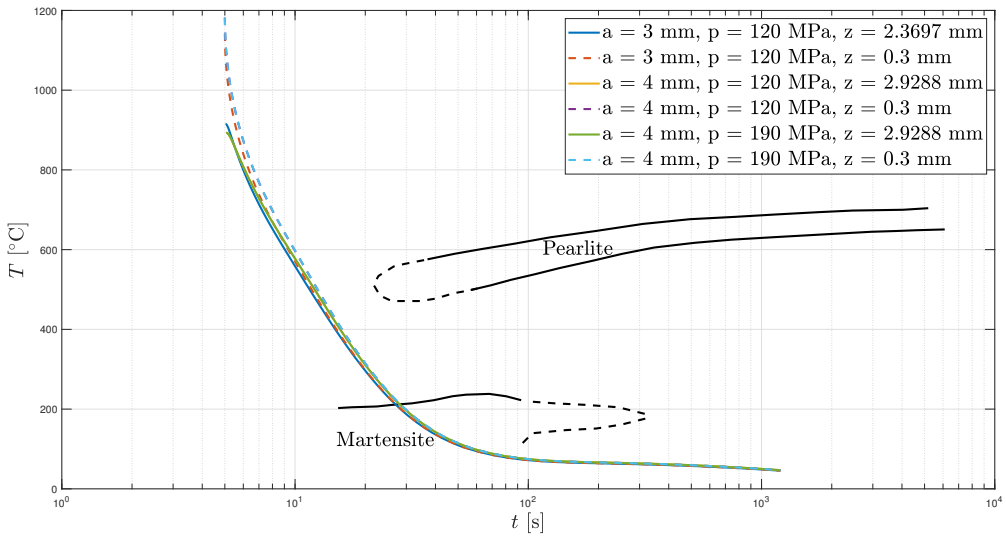

Figure 12: Comparison of welding parameters and z-coordinates for R260, second heat model, welding time 5 s and no preheating.

When investigating the effects of weld time and preheating, the cooling rate with respect to location in the HAZ was seen to be small. The fastest cooling rate was observed in the furthest direction from the weld surface into the specimen belonging to the HAZ, see Figure 3, where the direction into the specimen is shown with the z-direction from the surface. Therefore these points in the HAZ were used to investigate the cooling rates in the subsequent parameter tests.

Figure 13 shows the cooling rates for different welding times and preheating temperatures. Longer welding times and preheat temperatures make the cooling rate become slower, avoiding martensite. The purple and orange lines in Figure 13 are the best candidates for the welding of a pearlitic structure.

Figure 13 shows that the half width of the HAZ ranges from approximately 2.9 mm to 7.6 mm, which is in line with LFW experiments [6]. The width of the HAZ is seen to increase for longer welding times and higher preheat temperatures.

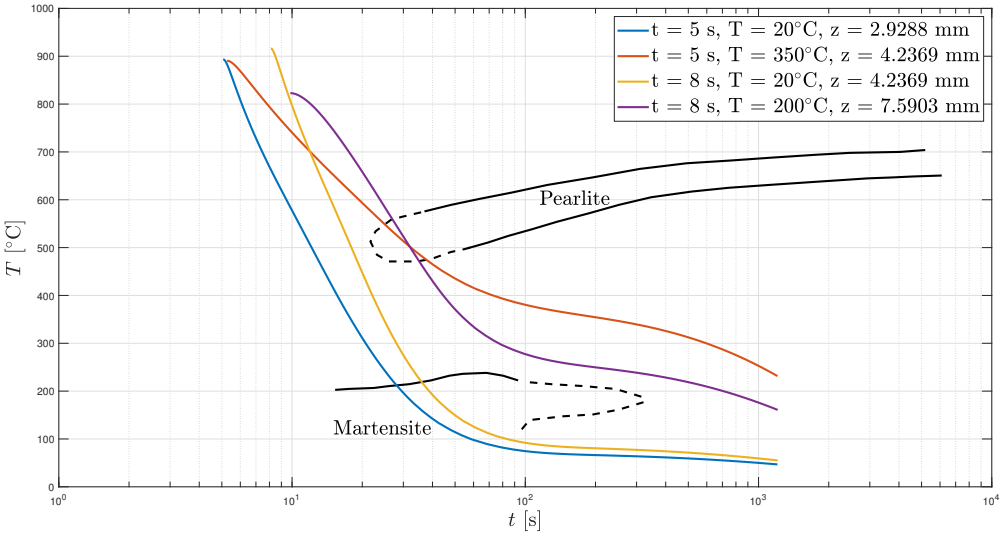

Figure 13: Comparison of welding times 5 s and 8 s, preheating to 200 °C and 350 °C, amplitude 4 mm and pressure 190 MPa.

3.4 Estimation of Microstructure for B360

The same conclusions which were made for R260 regarding the influence of amplitude and pressure parameters were also found for B360. The location used for all comparisons was again chosen as the largest z-coordinate in the HAZ for the same reason as with R260, Figure 3 shows z-direction. A comparison of welding parameters and z-coordinates is presented in Figure 14.

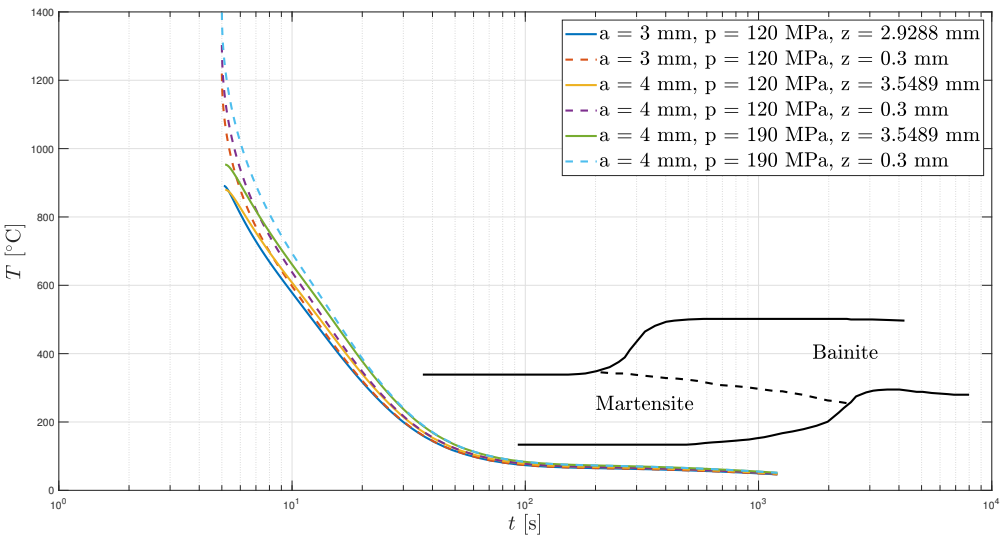

Figure 14: Comparison of welding parameters and z-coordinates for B360, heat model 2, welding time 5 s and no preheating.

The material properties chosen for B360 (S355JR) were compared with those for R260 and the results are shown in Figure 15, where the cooling rates are seen. As mentioned in section 2.2, the motivation for using S355JR was due to the similar metallurgical composition. The cooling rates for R260 and S355JR are very similar as seen Figure 15.

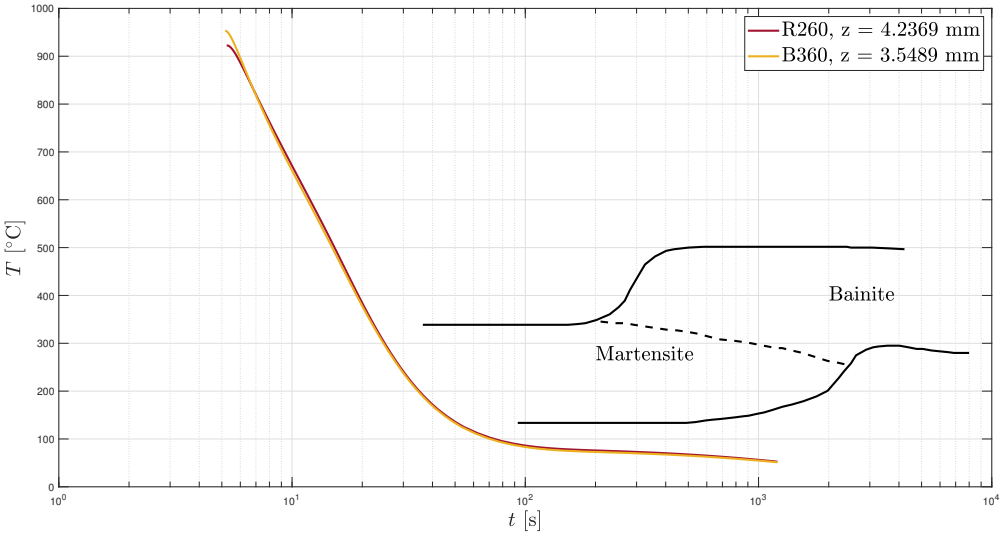

Figure 15: Comparison of material properties for R260 and B360 (S355JR), welding time 5 s, amplitude 4 mm and pressure 190 MPa.

In Figure 16 the cooling rates are shown for different welding times and preheat temperatures. The best candidate for obtaining bainitic structure is seen to be the parameter combination of a welding time of 5 s and a preheat of 350 °C.

Figure 16 shows that the half width of the HAZ ranges from approximately 3.5 mm to 5.75 mm. As with R260 this is in line with LFW experiments [6] and the width of the HAZ is again seen to increase for longer welding times and higher preheat temperatures.

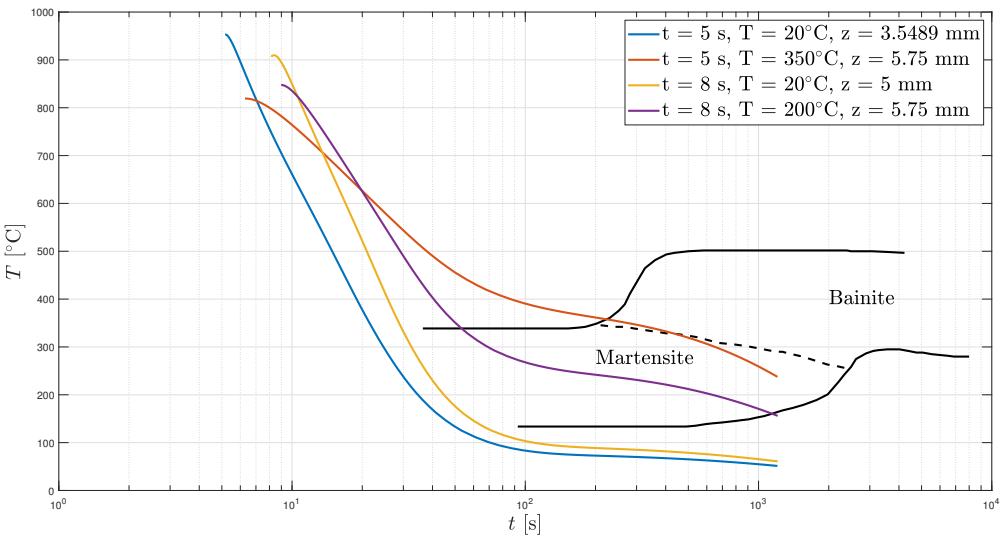

Figure 16: Comparison of welding times 5 s and 8 s, preheating to 200 °C and 350 °C, amplitude 4 mm and pressure 190 MPa.

4 Discussion

Heat model 2, which was used for parameter evaluation, gives a result that matches with experiments when no preheating is used. The experiments [6] have used parameters, as proposed by the WRIST project, and give a martensitic structure for both R260 and B360. The results from this study suggest that preheating is needed to achieve the desired microstructure, i.e. pearlitic for R260 and bainitic for B360.

The different welding parameters that have been investigated with respect to cooling rates have suggested some parameter combinations to achieve pearlitic and bainitic structure for the R260 and B360 materials respectively. Specifically larger heat inputs, in combination with a higher initial temperature for the specimen, result in lower cooling rates. The parameters giving larger heat input are larger welding time, preheating and increased oscillation amplitude and pressure.

For higher temperatures the friction coefficient is low due to low yield stress. Therefore an increase in pressure and oscillation amplitude will not increase the heat input further. These observations make the welding time and preheat most important for developing the desired microstructure.

To make it possible to arrive at a result for the project some simplifications were made in the modelling. The FEA used has been purely thermal which does not account for the material removal, i.e burn-off. However this is thought to be a minor effect since rather limited material is actually removed, i.e, the weld flash, see Figure 1b and secondly, the points selected for estimating cooling rates were outside the burn-off zone.

The parameters for surface convection were seen to have a small impact on the cool down in another railway welding experiment using thermite welding [14]. For B360, thermal material properties were taken from a material with similar material composition (S355JR), which could affect the result. The results from R260 and those from S355JR differed little which suggest they may be the same for the actual material data for B360.

Late in the project it was learned that only 7 mm of the specimen was outside the fixture [20], instead of 10 mm used. This information was given when the simulations were completed. This could affect the results somewhat since more material is in contact with the fixture. In addition the size and contact between specimen and fixture were initially unknown and were estimated by this project. A bigger fixture affects how much heat can be accumulated and might therefore give a faster cooling rate during microstructure formation.

5 Conclusions

The purpose of the study was two-fold: first to investigate whether or not LFW will result in a narrow HAZ and second to investigate whether or not LFW of B360, a bainitic steel, can produce a suitable microstructure in the HAZ providing superior properties to R260. The HAZ was found to be narrow, similar to results for LFW [6] and OFW [21].

When the provided welding parameters given by the WRIST project (Table 1) were combined with a welding time of 5 s it was found that the resulting microstructure was martensite for all parameter combinations. These results were later validated against LFW experiments, as those also showed formation of martensite.

Further, a preheat of the material and an extended welding time were included in the simulations. Using these welding parameters, it was shown that martensite formation is avoided for R260 while for B360 the microstructure will be a combination of martensite and bainite. In terms of contribution to the WRIST project a preheat and an extended welding time is suggested for R260 to investigate the impact on the microstructure.

6 Future Work and Recommendations

From this study it has clearly been found that the microstructure of the two different steels formed martensite after cooling without preheating the material. Preheating to 350 °C or increasing the welding time to 8 s and preheating to 200 °C resulted in a slower cool down for R260 and formation of martensite was avoided. In future experiments either of these setups for R260 is recommended to validate the obtained results for the FEA. For B360 has been found that neither of these measures will avoid completely formation of martensite. Preheating to 350 °C resulted in a material consisting of both martensite and

bainite. In this case a heat can be applied even in the cooling phase over a longer period of time so that the bainite has time to form. The heat can then be removed when the cooling rate curve has avoided the martensitic region in the CCT-diagram.

Mechanical deformations and burn-off, which creates weld flash, were not considered in this study. In order to get more realistic results from simulations, it is recommended to include these behaviours as they probably will affect the heating of the material. Two alternatives could be considered, first, in a thermal analysis, elements could be deleted as the welding proceeds and in that way moving the boundary where heat is applied. Alternatively, a full thermal-mechanical analysis in which the heat is generated through the pressure of the contact and the softer material is pushed out, could be used.

The thermal material properties provided by the WRIST project were limited for B360 and the thermal material properties of a surrogate material S355JR were used as an alternative. To increase the reliability of the simulations further investigation is recommended to improve the material data.

References

[1] Lonsdale, C."Thermite rail welding: History, process developments, current practices and outlook for the 21st century," Conrail Technical Services Laboratory Altoona, PA 16601, Tech. Rep., 1999.

[2] Bisschop, R."A guide to simulating aluminothermic welding of rails with finite elements," Chalmers University of Technology, Department of Industrial and Materials Science, Division of Material and Computational Mechanics, Tech. Rep., 2019.

[3] Vairis, A., Frost, M."High frequency linear friction welding of a titanium alloy," *Wear*, vol. 217, pp. 117–131, 1998.

[4] Vairis, A., Frost, M."On the extrusion stage of linear friction welding of Ti 6Al 4V," *Materials Science and Engineering A*, vol. 271, pp. 477–484, 1999.

[5] Faes, K."Investigation of the weldability of pearlitic and bainitic rail steels using linear and orbital friction welding," WRIST- EU project 626164, March 18, 2019, presentation at TRW meeting, Gent, Belgia.

[6] Faes, K., Maas, F."Deliverable D6.2: Influence of the process parameters on the joint properties," WRIST- EU project 626164, 2019.

[7] Josefson, B. L.Chalmers University of Technology, Dept. of Industrial and Materials Science, April 2, 2019, personal communication.

[8] Thorsell, C., Ringius, H."FE modeling of friction welding," Master's thesis, Chalmers University of Technology, 2017.

[9] Li, W., Vairis, A., Preuss, M., Ma, T."Linear and rotary friction welding review," *International Materials Reviews*, vol. 61, no. 2, pp. 71–100, 2016.

[10] M.TOMICIC-TORLAKOCIV"Guidelines for the rail grade selection," *Metalurgija -Sisak then Zagreb-*, vol. 53, 2014.

[11] Jauswal, J., Secordel, P., Fau, F."Corus premium grades to adress wear and rolling contact fatigue," Corus Rail, retrieved 2019-04-04. [Online]. Available: https://www.arema.org/files/library/2010_Conference_Proceedings/Corus_Premium_Grades_to_address_Wear_and_Rolling_Contact_Fatigue.pdf

[12] Interpretation of the microstructure of steels. University of Cambridge. [Online]. Available: https://www.phase-trans.msm.cam.ac.uk/2008/Steel_Microstructure/SM.html Retrieved 2019-05-19.

[13] Josefson, B. L., Brouzoulis, J., Maglio, M."Deliverable D4.1: Creation of a finite-element model of the orbital friction welding process – complement: Validation," WRIST- EU project 626164, 2018.

[14] Bisschop, R., Oddy, C."Log of thermal simulation-version 1," Chalmers University of Technology, Department of Materials and Industrial Science, Division of Material and Computational Mechanics, Tech. Rep., 2016.

[15] Bisschop, R., Granlund, M., Kalasho, K., Nordenskjöld, K."Finite element analysis on the application of an orbital friction welding process to rails," 2016, Report in Project in Applied Mechanics TME131.

[16] Bevan, A., Jaiswal, J., Smith, A., Cabral, M. O."Judicious selection of available rail steels to reduce life cycle costs," Institute of Railway Research, University of Huddersfield, Huddersfield, Queensgate and Institute of Transport Studies (ITS), University of Leeds, Leeds, Tech. Rep., 2018.

[17] Chen, Y., Lawrence, F., Barkan, C. P. L., Dantzig, J. A."Heat transfer modelling of rail thermite welding," *IMechE Journal of Rail and Rapid Transit*, vol. 220, pp. 207–217, 2006.

[18] Josefson, B. L., Alm, J., McDill, J. M. J."Simplified FEA models in the analysis of the redistribution of beneficial compressive stresses in welds during cyclic loading," in *Procedings of the 37th International Conferece on Offshore Mechanics and Arctic Engineering-OMAE, Madrid, Spain*, no. OMAE2018-77401, June 2018.

[19] "Eurocode 3: Design of steel structures, part 1.2 : Structural fire design, brussels," EN1993-1-2 European Committee for Standardisation (CEN), 1993.

[20] Maas, F.Belgian Welding Institute, April 4, 2019, personal communication.

[21] Maas, F., Faes, K."Deliverable D5.3: Report with the measured joint properties and materials and dimensions of the intermediate components," 2019, WRIST- EU project 626164.

[22] "Structural welding code–steel," 1999, American National Standard: AWS D1.1:2000.

[23] Steels – carbon steels, mild steel, carbon-manganese steels, alloys steels, low-alloy steels and micro-alloy steels. AZoM. [Online]. Available: https://www.azom.com/article.aspx?ArticleID=2537 Retrieved 2019-05-19.

A FORTRAN code

```
C       HEAT FLUX CALCULATION FOR HEAT MODEL 1

        SUBROUTINE DFLUX(FLUX,SOL,KSTEP,KINC,TIME,NOEL,NPT,COORDS,JLTYP,
     1        TEMP,PRESS,SNAME)
        INCLUDE 'ABA_PARAM.INC'
        DIMENSION FLUX(2), TIME(2), COORDS(3)
        REAL*8 MU, P, V
        REAL*8 AA, BB, CC
        CHARACTER*80 SNAME

        AA = 0.142186d0
        BB = 0.466507d0
        CC = -0.003156d0
        V = 0.48d0
        P = 120000000d0

C       MU CALCULATION

        MU = AA*(SOL**BB)*(EXP(CC*SOL))

C       HEAT FLUX CALCULATION
        FLUX(1) = (MU*P*V)
        FLUX(2) = 0.0d0


        RETURN
        END

C       HEAT FLUX CALCULATION FOR HEAT MODEL 2

        SUBROUTINE DFLUX(FLUX,SOL,KSTEP,KINC,TIME,NOEL,NPT,COORDS,JLTYP,
     1        TEMP,PRESS,SNAME)
        INCLUDE 'ABA_PARAM.INC'
        DIMENSION FLUX(2), TIME(2), COORDS(3)
        REAL*8 MU, P, V, SIGMAY, SIGMAYZERO, TZERO
        REAL*8 SIGMAYSLOPEONE, SIGMAYONE, TONE, SIGMAYSLOPETWO
        REAL*8 AA, BB, CC
        CHARACTER*80 SNAME

        AA = 0.142186d0
        BB = 0.466507d0
        CC = -0.003156d0
        V = 0.48d0
        P = 120000000d0
        SIGMAYZERO = 430000000d0
        TZERO = 400d0
        SIGMAYSLOPEONE = -956750d0
        SIGMAYONE = 47300000d0
        TONE = 800d0
        SIGMAYSLOPETWO = -93250d0

C       MU CALCULATION

        MU = AA*(SOL**BB)*(EXP(CC*SOL))
```

```
C       SIGMAY CALCULATION

        IF(SOL .LT. TZER0) THEN
         SIGMAY = SIGMAYZERO
        ELSEIF(SOL .LT. TONE) THEN
         SIGMAY = SIGMAYZERO+SIGMAYSLOPEONE*(SOL-TZERO)
        ELSE
         SIGMAY = SIGMAYONE+SIGMAYSLOPETWO*(SOL-TONE)
        ENDIF

C       HEAT FLUX CALCULATION

        IF(MU*P .LT. SIGMAY/SQRT(3d0)) THEN
         FLUX(1) = (MU*P*V)
         FLUX(2) = 0.0d0

        ELSE
         FLUX(1) = (SIGMAY/SQRT(3d0)*V)
         FLUX(2) = 0.0d0

        ENDIF

        RETURN
        END
```